Applied Physics A (2023) 129:451
https://doi.org/10.1007/s00339-023-06730-x

Applied Physics A
Materials Science & Processing

The electronic and magnetic properties of the bulk, Sc_2MnSi surfaces, and Sc_2MnSi/CdTe (111) interface

Mudhahir H. Jolan[1] · **Jabbar M. Khalaf Al-zyadi**[1]

Received: 9 February 2023 / Accepted: 19 May 2023 / Published online: 31 May 2023

Abstract
In this work, the electronic and magnetic features of the Sc2MnSi bulk, surfaces, and the interface with the semiconductor CdTe (111) were thoroughly researched using the first-principles calculations. The Sc_2MnSi alloy with equilibrium lattice constant of 6.34 Å shows half-metallic (HM) property. This alloy exhibits an energy gap and a HM gap of 0.54 and 0.12 eV, respectively. The density of states results confirm the existence of the half-metallicity property for the Sc_2MnSi component at SiSc(2)-(001), Sc(2)-, and Si-(111) surfaces while this property is not revealed at Sc(1)-, Mn-terminated (111), Sc(1)Mn-terminated (001), and Sc_2MnSi (110) surfaces for the same component. In addition, in the case of Sc_2MnSi/CdTe interface, it is noted that Cd-Si connection does not reveal the half-metallicity feature, while the Si-Te shape exhibits a 100% spin polarization, thus preserving the half-metallicity. Furthermore, the Si-Te shape is more stable than the others, according to the interfacial adhesion energy.

Keywords Sc_2MnSi full Heusler compound · Half-metallic · Electronic structure · Surface and interface properties · Density functional theory

1 Introduction

The basis formation of magnetic tunneling junction is achieved when an insulator or a thin semiconductor is sandwiched between two particular metal layers. The tunneling current is typically higher depending on the value of the magnetic moment. Building the magnetic tunneling devices open the door for many applications in sensors devises based on the magnetic [1], reading heads in hard disk drives [2, 3], magnetic random-access memories [4], and many other spintronics applications [6-8]. To optimize the performance of magnetic tunneling junction, the percentage of one of the important parameters, such as Tunnel Magnetoresistance (TMR) should be increased. For the two ferromagnetic metals, the ratio of TMR is defined by the Julliere formula of the spin polarization P [8]. The high values of TMR can be achieved by increasing the P values of the heterojunctions layers in the metal/semiconductor according to equation $\mathrm{TMR} = 2P_1P_2/(1 - P_1P_2)$. Anyway, the presence of the Half-Metallic (HM) characteristic in the bulk does not mean that it is also present in the surfaces or interfaces, because there are a lot of anti-polarizing elements, such as non-arrangement of atoms [9, 10], surface states [11], interface states [12], magnetic exchange coupling in the interface [13], and thermal factors [14–16], for these reasons, researchers focus on the bulk, surfaces and interfaces of Heusler alloys. The general chemical formula of the Heusler alloys are taken the form X_2YZ, where X and Y are transitional elements, while Z is the main group element, in Wyckoff coordinates if the positions of the atoms X (1 and 2) at A (0, 0, 0) and C (1/2, 1/2, 1/2), Y at B (1/4, 1/4, 1/4), while Z at D (3/4, 3/4, 3/4) locations, this arrangement of the sites can form the ordinary full Heusler alloy of the composition $AlCu_2Mn$ ($L2_1$), with space group (No. 225, Fm-3m). Meanwhile, if the positions of the X (1 and 2) and Y atoms change to A (0, 0, 0), B (1/4, 1/4, 1/4), C (1/2, 1/2, 1/2), respectively, and the Z atoms remain in the same positions D (3/4, 3/4, 3/4), such an arrangement is called the Heusler alloys of the composition $CuHg_2Ti$ ($C1_b$), with space group (No. 216, F43m) as the prototype is noticed [17]. Recent studies have confirmed the presence of HM properties in new Heusler compounds, for example; Mn_2CoZ (Z = Ge, Ga, Al, Bi, As and Sb) [18], Mn_2TiZ (Z = Ge, Ga, Al, Bi, As, Sb, Sn and Si) [19], Fe_2YSi

✉ Jabbar M. Khalaf Al-zyadi
jabbar.khalaf@uobasrah.edu.iq; jabbar_alzyadi@yahoo.com

[1] Department of Physics, College of Education for Pure Sciences, University of Basrah, Basrah 6100, Iraq

(Y = Cr and Mn) [20], Fe_2MnP [21], Fe_2TiP [22], Cr_2MnZ (Z = As, Al, Bi, Sb, Bi, and P) [23, 24]. Therefore, the thin films or multiple layers based on HM materials is used in many spintronics devices, therefore, it is important to investigate the characteristic of surfaces and interfaces [25–29]. Two-dimensional materials optical and electronic features have been thoroughly highlighted [30–36].

In this paper, the electronic and magnetism properties of the Sc_2MnSi compound in $CuHg_2Ti$-type, and (111), (001), and (110) surfaces, and interface Sc_2MnSi/CdTe are studied using the investigation of first-principle calculation.

2 Computational methods

To calculate the electronic and magnetic properties of the Sc_2MnSi Heusler alloy, the first-principles method is investigated based on the DFT that applied by Wien2k [37]. In the bulk Sc_2MnSi Heusler alloy the meshes k-point is $(12 \times 12 \times 12)$, while the meshes are $(12 \times 12 \times 1)$ and $(8 \times 12 \times 2)$ for the (111), (001), and (110) surfaces, respectively. The value of energy convergence is (10^{-5} Ry). The smaller radius of muffin-tin sphere R_{MT} are determined for the atoms Sc = Mn = 2.50 a.u and Si = 2.39 a.u.. The plane wave has a cut-off energy parameter $K_{max}R_{MT}$ equal to 8, where K_{max} is the largest value of the reciprocal lattice vector. Inside the atomic sphere, the angular momentum has a maximum value l_{max} equal to 10. Additionally, the based on spin results, the initial spin shapes of Sc_2MnSi are calculated to be ferromagnetic (spin in one orientation, down or up, and the material has spin magnetic moment), nonmagnetic (not spin), and antiferromagnetic (spin down = spin up, and the spin magnetic moments equal zero), demonstrating that Sc_2MnSi is a ferromagnetic material. The valence electrons of the Sc_2MnSi compound are Sc1 ($4s^2$, $3d^1$), Sc2 ($4s^2$, $3d^1$), Mn ($4s^2$, $3d^5$), and Si ($3s^2$, $3p^2$).

3 Results and discussion

3.1 Electronic properties

To search the electronic properties of Sc2MnSi Heusler alloy, the equilibrium lattice constant will be calculated by finding the Sc_2MnSi total energies as a function of the lattice parameters. It is noted that the lowest value of energy is located at 6.34 Å, which is consistent with theoretical studies [38]. As shown in Fig. 1, the energy gap in the spin-up channel crosses energy bands in the spin-down channel, where the Fermi level is located in the middle. Therefore, the band structures of Sc_2MnSi compound show that the HM has an indirect energy and (HM) gaps of 0.54 and 0.12 eV, respectively. The (HM) gap is the least energy needed to convert the spin up of valence band electrons close to the E_F to the minority spin.

Finally, Skaftouros et al. [39] have presented very necessary notes about the resulting hybridization between d-orbitals of metal elements in the form of the Heusler compound, for instant, Sc-based Heusler alloys. This means that the similarity between the X1 and the Y atoms lead to that their d-orbitals hybridize with each other exhibit five bonding d ($2e_g$ and $3t_{2g}$) and non-bonding ($2e_u$ and $3t_u$). After that, the five X1–Y bonding d states hybridize together with the d-orbitals of the X2 atoms and produce bonding and anti-bonding states after then. As shown in Fig. 2, in the $CuHg_2Ti$-structure, the energy bands under

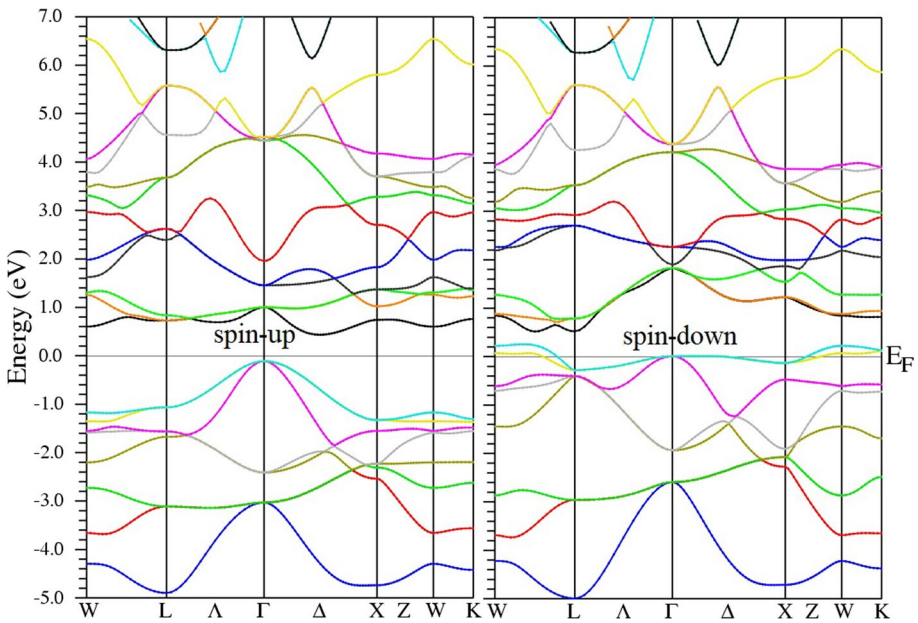

Fig. 1 Band structure of Sc_2MnSi Heusler alloy. The zero energy is set to E_F

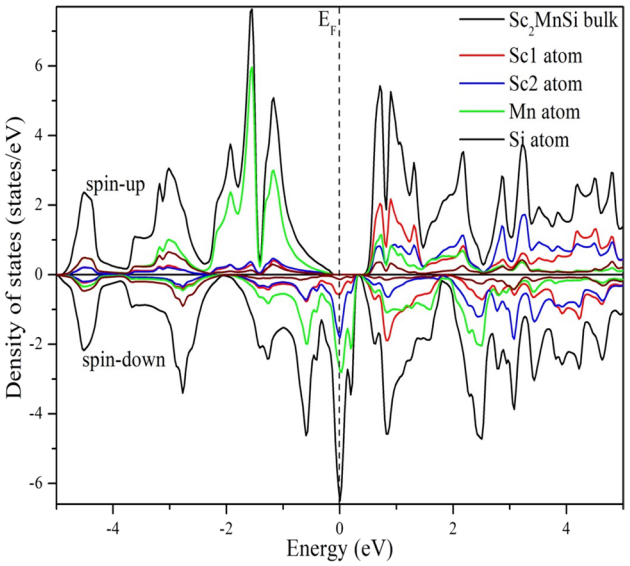

Fig. 2 The bulk density of states for Sc_2MnSi

the E_F in spin-up channel over the range from − 2.5 to 0.0 eV are often attributed to bonding states. While the bands between 0 and 3 eV up the Fermi level represent non-bonding states ($2e_u$ and $3t_u$) and the high energy bands between 3 and 6 eV are represent anti-bonding states. The energy of the three bands are evaluated between − 5.0 and − 2.5 eV attributed to p orbital of Si and the isolated energy band located close to − 9.0 eV is attributed to Si s states. The influence of splitting exchange on spin down channel leads to the bonding states rushing towards and crosses the Fermi level.

3.2 Magnetic properties

Spinning splitting of 3d orbitals into majority-spin and minority-spin states of the DOS at E_F leads to the presence of magnetic properties in the compounds, that is why we study the Sc_2MnSi Heusler alloy, which features 3d transitional elements (Sc and Mn), where the results proved that the Sc_2MnSi is subject to the rule of Slater–Pauling $M_t = 18 - Z_t$, where M_t represents the spin magnetic moment and Z_t represents the valence electrons Sc1: $4s^2$ $3d^1$, Sc2: $4s^2$ $3d^1$, Mn: $4s^2 3d^5$, and Si: $3s^2 3p^2$, which are 17 electrons in the Sc_2MnSi compound. Thus, the total magnetic moment is determined to be $1\mu_B$. The magnetic moments of atoms are − 0.486, − 0.373, 2.093, and − 0.048 μ_B for Sc1, Sc2, Mn, and Si atoms, respectively and − 0.186 μ_B of the interstitial area, as listed in Table 1. The Mn and Si atoms have the greatest and small contributions to forming the spin magnetic moment.

3.3 Surfaces relaxation and structural properties

To study the surface properties Sc_2MnSi based on the equilibrium lattice constants for the (111), (001), and (110) surfaces, a slab with 25, 13, and 7 atomic layers could be constructed, respectively. These slabs would then have a 15 vacuum added to them. It is determined that the chosen slabs' thickness is adequate for studying the surface characteristics. It is noteworthy that each layer of (111) surface contains only one atom, therefore, there are four different layers of the (111) surface, which are Sc1-, Sc2-, Mn-, and Si-terminations, while there are two layers of the (001) surface, layer has the termination Sc1Mn-, and the other layer has the Sc2Si-termination. The Sc1Sc2MnSi-termination is the only termination on the (110) surface that maintains the four atoms together. To assure the stability of surface structures, the top four atomic layers of the slabs were allowed to relax, while the other atomic layers were maintained in place by a reduction in the overall energy and atomic interaction forces. The process of relaxation layers and the number of its slabs is sufficient to exam the surface properties because of the small amount of change in the magnetic moment and the bond length (particularly smaller than 0.0015 μ_B and 0.003 Å, respectively). To ensure the stability of the surfaces, the distances between the atoms after and before relaxation are calculated, where the results showed before relaxation that the distance between the atoms of the (111) surface and the subsurface is 2.745 Å for the Sc1, Sc2-, Mn-, and Si-terminations. On the other hand, after relaxing the distance becomes 2.781, 2.893, 2.688, and 2.650 Å for Sc1-, Sc2-, Mn-, and Si-terminations, respectively. This indicates an increase in the bond length with respect to the Sc1- and Sc2-terminations, on contrary, it decreases with respect to the Mn- and Si-terminations, as for the Sc1Mn- and Sc2Si-(001) surfaces, before relaxation, there is a 2.745 separation between the surface and the subsurface, after relaxation are 2.911 and 2.891 Å, respectively. After relaxation, the distance between the Sc1 surface atom and the Sc2 subsurface atom is 2.869 Å, while the distance between the Mn surface atom and the Si subsurface atom is 2.537 Å, resulting in the Sc1Mn-termination. In contrast, the Sc2Si-termination following relaxing has a distance of 2.534 Å between the Si surface atom and the Mn subsurface atom and a distance of 2.891 Å between the Sc2 surface atom and the Sc1 subsurface atom. This means that for both the (111) and (001) surfaces, the Mn and Si surface atoms are migrating towards the center while the Sc1 and Sc2 surface atoms are traveling towards the vacuum. Before relaxing, the distance between the surface atoms and the subsurface atoms with respect to the (110) surface is 3.17 Å, and after relaxation, it becomes 4.998, 3.334, 2.835 and 2.941 Å, for Sc1, Sc2, Mn, and Si, respectively. This indicates that although the Mn and Si surface atoms are migrating toward the center of

Table 1 The atoms magnetic moments in the Sc_2MnSi full Heusler alloy of the bulk, surfaces, and subsurfaces. Additionally, the values of the atoms' computed spin polarization are displayed

	Atom	s (↑/↓)	p (↑/↓)	d (↑/↓)	Total (↑/↓)	M (μ_B)	P (%)
Bulk	Sc1	1.08/1.11	3.05/3.08	0.42/0.76	4.57/4.97	−0.41	100
	Sc2	1.10/1.13	3.04/3.04	0.45/0.79	4.61/4.98	−0.37	100
	Mn	0.20/0.18	3.22/3.20	3.8/1.62	7.12/5.02	2.09	100
	Si	0.54/0.54	0.75/0.78	0.05/0.08	1.36/1.41	−0.05	100
Sc1-ter (111)	Sc1 (S)	1.08/1.11	3.01/3.01	0.41/0.64	4.77/4.41	−0.25	2.30
	Sc2 (Sub1)	1.12/1.13	3.03/3.02	0.54/0.66	4.71/4.83	−0.12	35.09
	Mn (Sub2)	0.22/0.19	3.20/3.18	3.74/1.54	7.17/4.93	2.25	70.00
	Si (Sub3)	0.53/0.52	0.72/0.75	0.5/0.08	1.32/1.36	−0.04	40.56
Sc2-ter (111)	Sc2 (S)	1.05/1.06	2.96/2.95	0.36/0.53	4.37/4.56	−0.17	100
	Mn (Sub1)	0.17/0.15	3.14/3.10	3.49/1.63	6.81/4.89	1.93	100
	Si (Sub2)	0.50/0.50	0.65/0.66	0.05/0.06	1.22/1.23	−0.02	100
	Sc1 (Sub3)	1.05/1.07	2.98/3.00	0.37/0.65	4.42/4.73	−0.30	100
Mn-ter (111)	Mn (S)	0.16/0.12	3.09/3.06	4.04/0.94	7.30/4.13	3.17	80.16
	Si (Sub1)	0.47/0.47	0.62/0.64	0.04/0.04	1.15/1.17	−0.03	21.97
	Sc1 (Sub2)	1.04/1.05	2.96/2.97	0.37/0.58	4.38/4.62	−0.23	73.92
	Sc2 (Sub3)	1.05/1.07	2.95/2.95	0.36/0.69	4.38/4.71	−0.33	89.41
Si-ter (111)	Si (S)	0.44/0.43	0.58/0.56	0.02/0.02	1.04/1.02	0.02	100
	Sc1 (Sub1)	1.07/1.07	3.01/3.01	0.42/0.56	4.52/4.66	−0.15	100
	Sc2 (Sub2)	1.07/1.09	3.03/3.03	0.44/0.56	4.56/4.69	−0.14	100
	Mn (Sub3)	0.19/1.16	3.19/3.15	3.72/1.44	7.11/4.77	2.33	100
Sc1Mn-ter(001)	Sc1 (S)	1.05/1.07	2.97/2.98	0.27/0.63	4.30/4.68	−0.38	48.53
	Mn (S)	0.20/0.17	3.13/3.11	3.90/1.24	7.24/4.53	2.70	46.69
	Sc2(Sub1)	1.08/1.10	2.99/3.00	0.40/0.72	4.49/4.82	−0.34	40.05
	Si (Sub1)	0.43/0.47	0.61/0.63	0.05/0.06	1.13/1.16	−0.03	19.75
	Mn (C)	0.16/0.15	3.16/3.15	3.60/1.54	6.93/4.84	2.09	100
	Sc1 (C)	1.06/1.08	3.00/3.02	0.37/0.70	4.44/4.81	−0.40	100
Sc2Si-ter(001)	Sc2 (S)	1.08/1.10	3.01/3.02	0.41/0.60	4.50/4.73	−0.23	100
	Si (S)	0.49/0.48	0.63/0.60	0.03/0.04	1.16/1.13	0.03	100
	Mn (Sub1)	0.21/0.18	3.23/3.20	3.82/1.46	7.27/4.86	−0.28	100
	Sc1 (Sub1)	1.09/1.11	3.06/3.08	0.51/0.71	4.67/4.91	2.40	100
	Si (C)	0.47/0.46	0.61/0.63	0.04/0.06	1.13/1.16	−0.05	100
	Sc2 (C)	1.10/1.13	3.04/3.04	0.45/0.79	4.61/4.99	−0.37	100
Sc_2MnSi-ter(110)	Si (S)	0.43/0.43	0.45/0.51	0.03/0.03	0.92/0.98	−0.06	17.38
	Mn (S)	0.19/0.16	3.14/3.11	3.74/1.40	7.09/4.68	2.40	67.21
	Sc1 (S)	1.06/1.07	2.96/2.96	0.37/0.56	4.40/4.60	−0.20	70.88
	Sc2 (S)	1.05/1.06	2.97/2.98	0.35/0.53	4.38/4.57	−0.20	38.05
	Sc1 (Sub1)	0.18/0.16	3.13/3.11	4.10/0.98	7.42/4.26	3.16	49.97
	Sc2 (Sub1)	0.42/0.42	0.43/0.46	0.03/0.03	0.88/0.91	−0.03	5.55
	Si (Sub1)	1.09/1.09	2.98/3.00	0.49/0.68	4.57/4.78	−0.21	27.50
	Mn (Sub1)	1.08/1.09	3.00/3.01	0.61/0.61	4.70/4.72	−0.01	17.05

the (110) surface, the Sc1 and Sc2 surface atoms are going toward the vacuum. To argue the surface half-metallicity, the surface and subsurface atomic partial and total DOS of the four possible (111), two possible (001), and one possible (110) surface for Sc_2MnSi are presented in Figs. 3, 4, 5, 6, 7, 8, 9 and 10. Testing the electronic structural differences between surfaces and bulk systems, the corresponding DOS in bulk structure are also provided simultaneously. The Sc2, Si, and Sc2Si-terminated surfaces appear to retain the HM characteristic of the bulk system pertaining to the electronic structure of surface depicted in Figs. 4, 6, and 8, with the exception of the reduction of energy gaps, i.e., the spin↑ channels are metallic, whereas there is an energy gap around the E_F for the spin↓ channels. The spin-up electrons have energy gaps for the (111) surface atoms of Sc2 and Si (0.11 and 0.46 eV), but the energy gaps for the (001) surface atoms of Sc2 and Si (0.36 and 0.30 eV) are elevated compared to the bulk values (0.59 and 0.57 eV). However, the

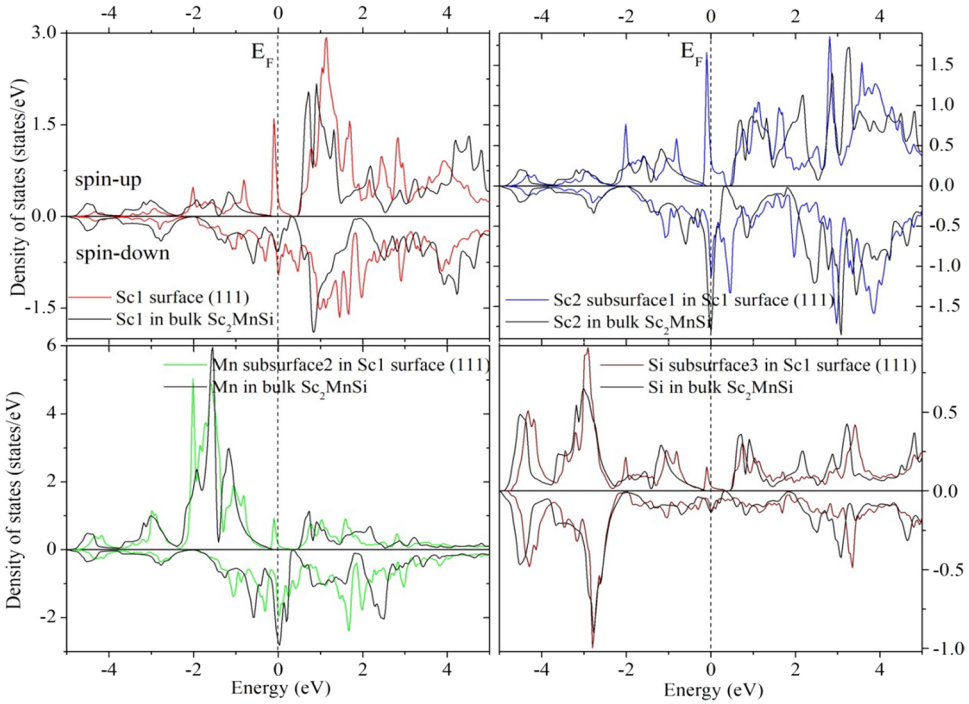

Fig. 3 DOS of the surface, subsurface atoms for Sc1-termanted, and Sc_2MnSi bulk. The Fermi levels are highlighted in the dashed line at 0 eV

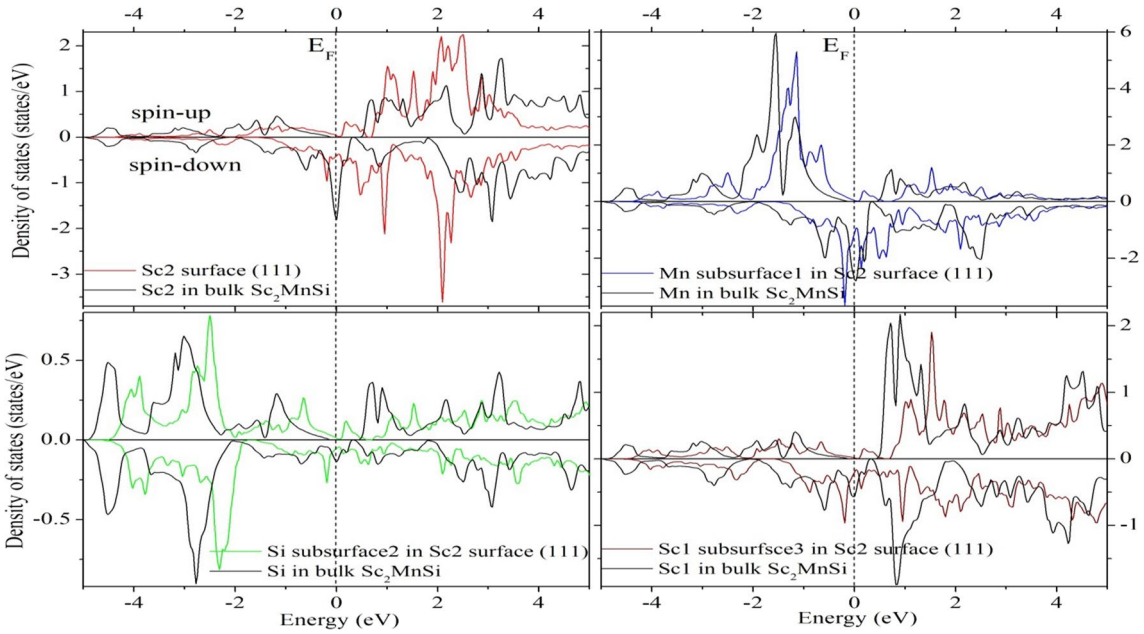

Fig. 4 Similar Fig. 3 but for Sc2-termanted surface

HM characteristics are not present at the Sc1-, Mn-, Sc1Mn-, and Sc1Sc2MnSi-terminated surfaces. This is because the possibility of multiple surface effects being caused by the decrease in atomic coordination numbers at surfaces, it is important to note that the genesis of surface states induced in the four surface structures. To better comprehend the surface electronic and magnetic characteristics, we further calculate the atoms magnetic moments (M μ_B) in the Sc_2MnSi full Heusler alloy for bulk, surfaces, and subsurface, which are listed in Table 1, along with the corresponding values of spin polarization calculation. It is demonstrated that all of the central-layer atoms on every surface have magnetic moments that are almost identical to those of the bulk structure. The fact that the atomic magnetic moments at the slab's center

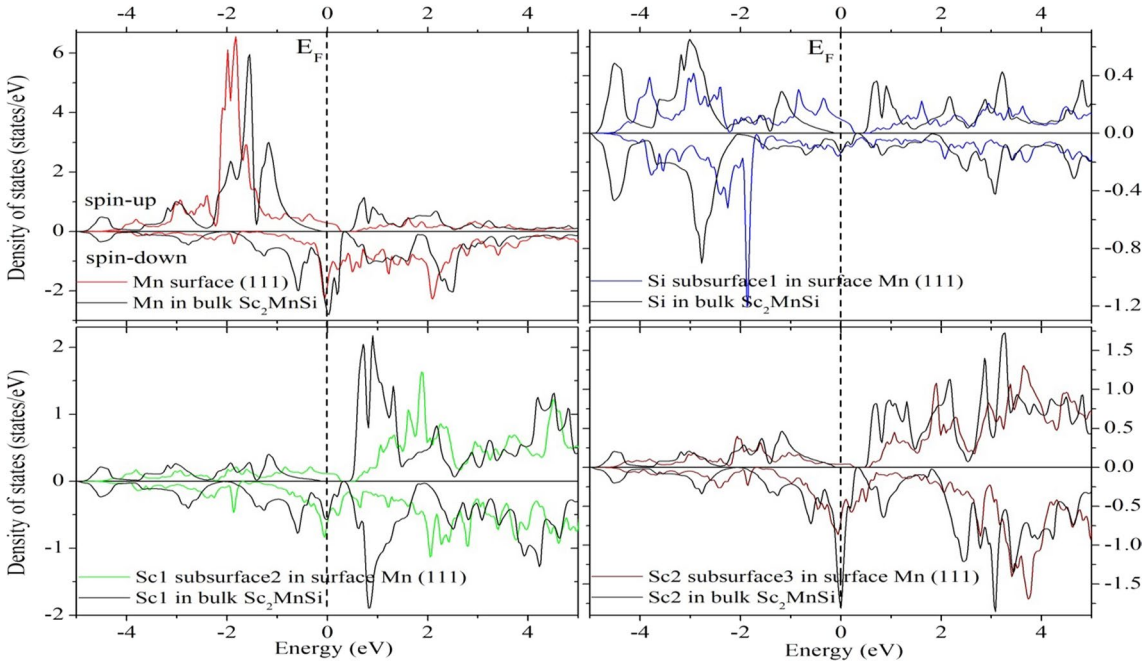

Fig. 5 Similar Fig. 3 but for Mn-termanted surface

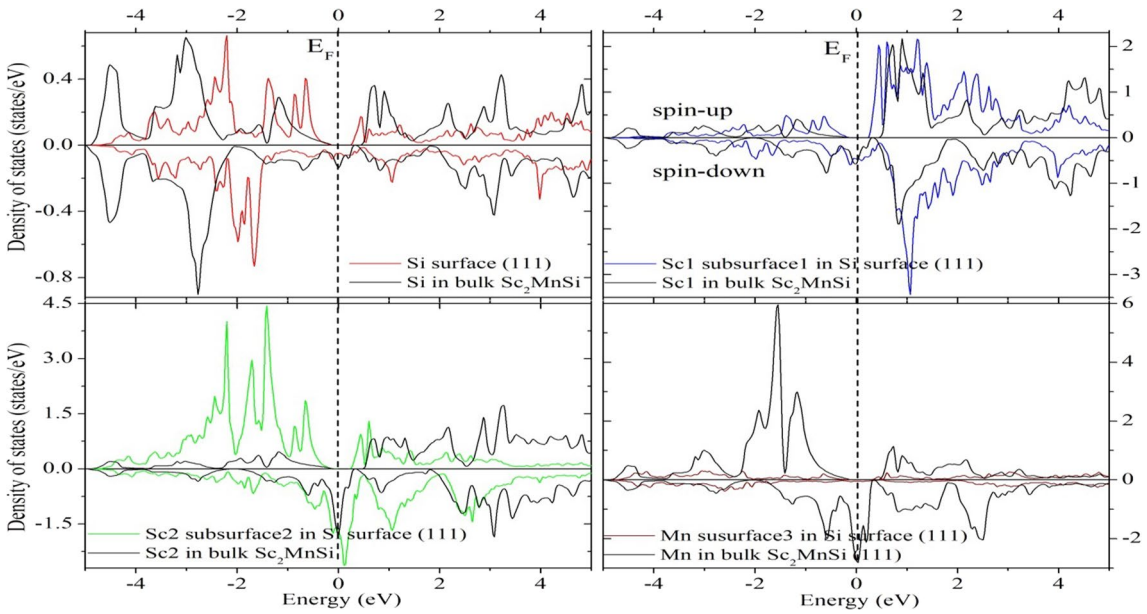

Fig. 6 Similar Fig. 3 but for Si-termanted surface

layer and in the bulk system are equal further proves that the slab we chose is reasonable. The magnetic moments of the Mn and Si atoms at the surfaces are increased, while the values of the Sc1 and Sc2 atoms at the surfaces are decreased compared to those in the bulk system due to the reduction of coordination number (the environment in the bulk Sc_2MnSi and its surface are quite different). Additionally, the spin polarization was determined as represented in Table 1 using the formula $P=(N\uparrow -N\downarrow)/(N\uparrow +N\downarrow)$, where $N\uparrow$ and $N\downarrow$ are the majority-spin and minority-spin dependent DOS at Fermi level, respectively. The 100% spin polarized both Sc2- and Si-terminated (111) surface structures and Sc2Si (001) surfaces are preferable for spintronic devices applications.

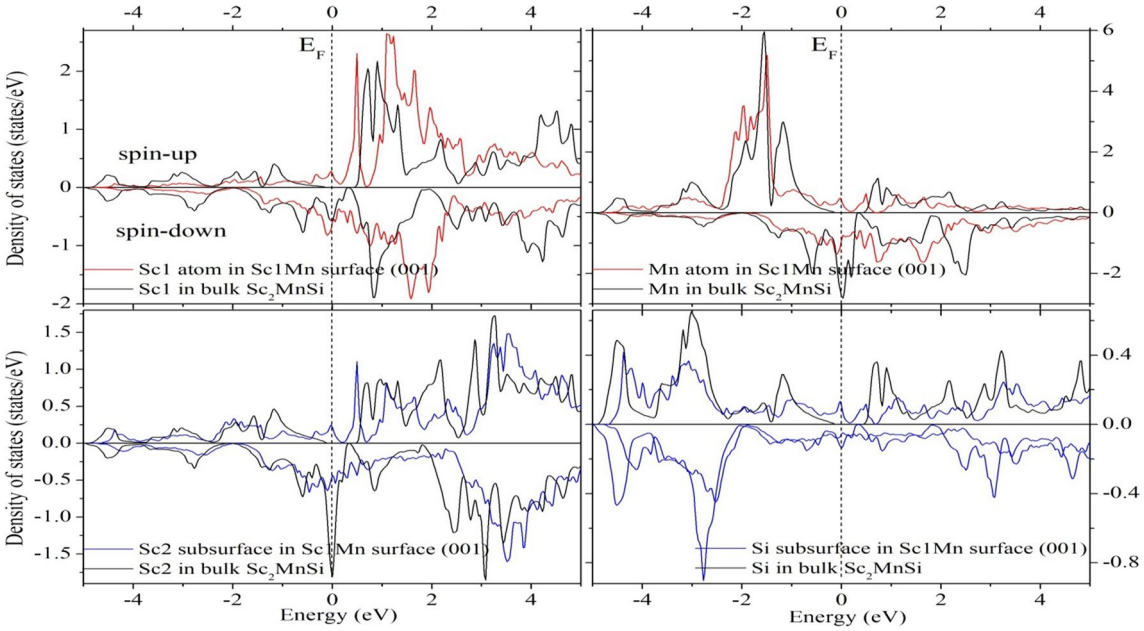

Fig. 7 The DOS of Sc_2MnSi (001) surface with the Sc1Mn-termination

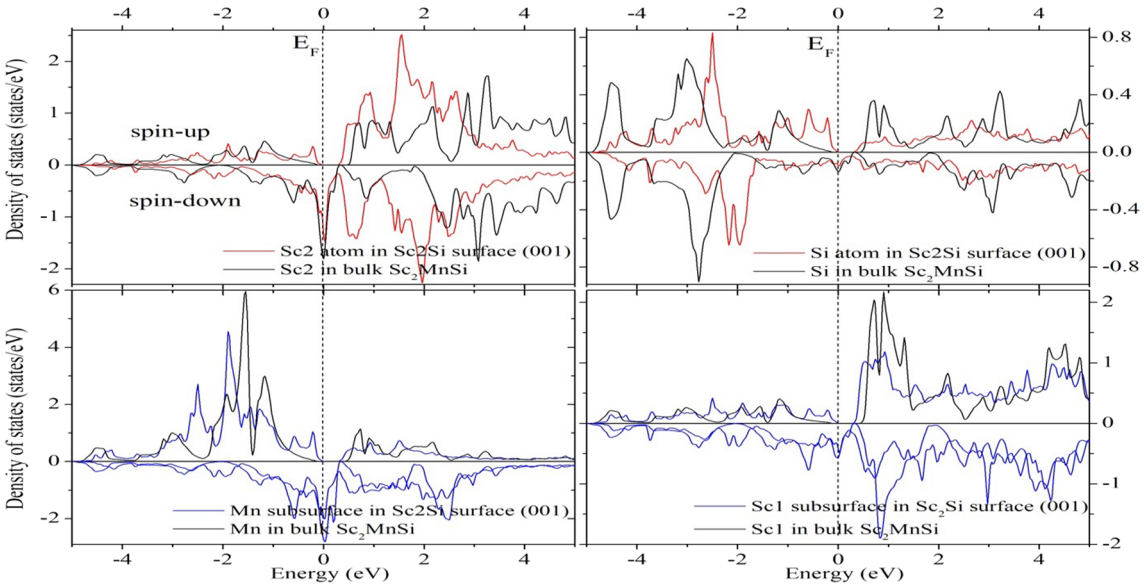

Fig. 8 Similar Fig. 7 but for Sc2Si-termanted (001) surface

3.4 Electronic and magnetic characteristics of the Sc_2MnSi/CdTi (111) interface

In this section, the interface effects on the electronic and magnetic features of the Sc_2MnSi/CdTi (111) interfaces are revealed. The PDOS for both interface and sub-interface atoms are studied for the two interfacial structures. For comparison, the PDOS nearby to the bulk are plotted. It is clear from Fig. 11 that the Si-Te interface presents the half-metallicity. This is because the spin-down channel shows the metallic characteristics since the spin-down electrons cross the Fermi level, while the spin-up channel shows semiconducting characteristics at the Fermi level (E_F). The energy and half-metal gaps in the spin-up channel were calculated to be 0.2 and 0.07 eV for Si atom, whereas for Te atom at Si-Te shape, the energy and half-metal gaps are 0.22 and 0.06 eV, respectively. While the Si-Cd interface disappear the half-metallicity of the bulk Sc_2MnSi due to

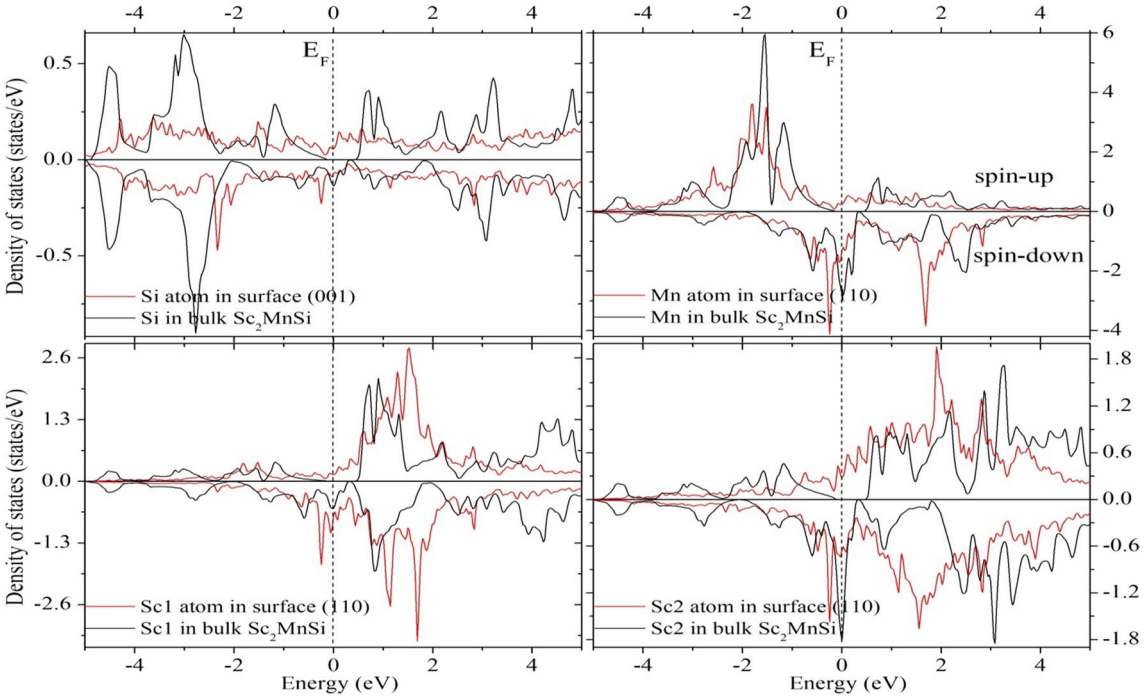

Fig. 9 The DOS of Sc_2MnSi (110) surface with the Sc1Sc2MnSi-termination

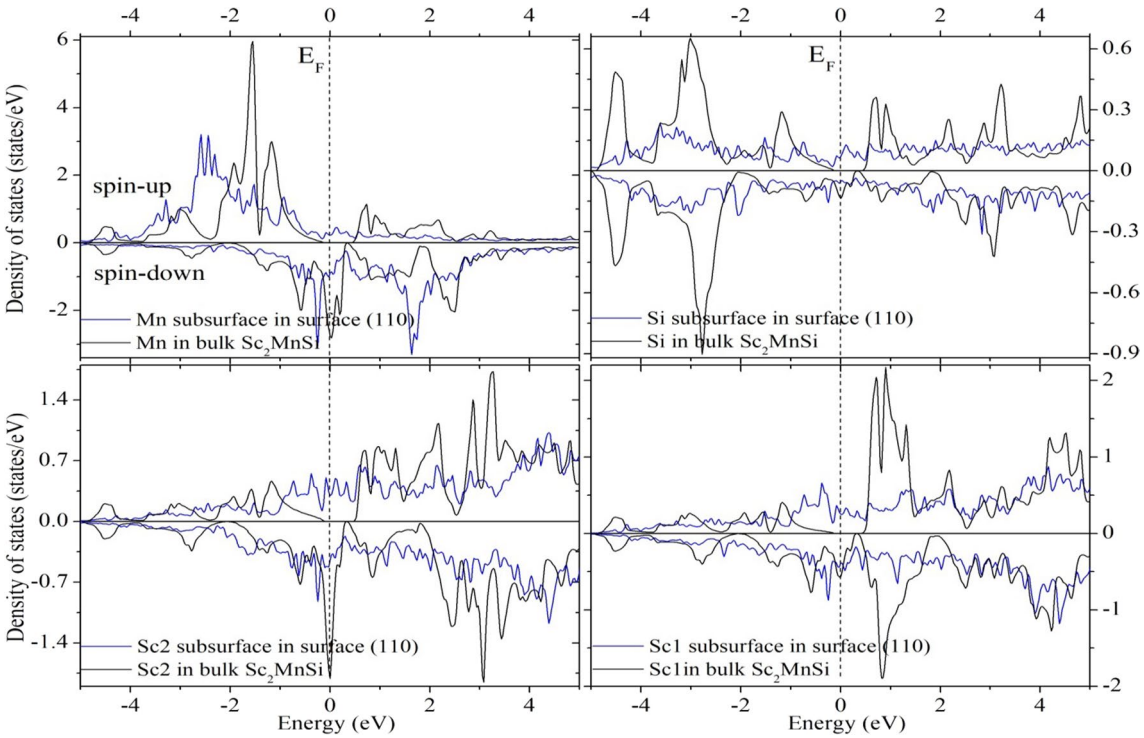

Fig. 10 Similar Fig. 9 but for Sc_2MnSi (110) subsurface with the Sc1Sc2MnSi-termination

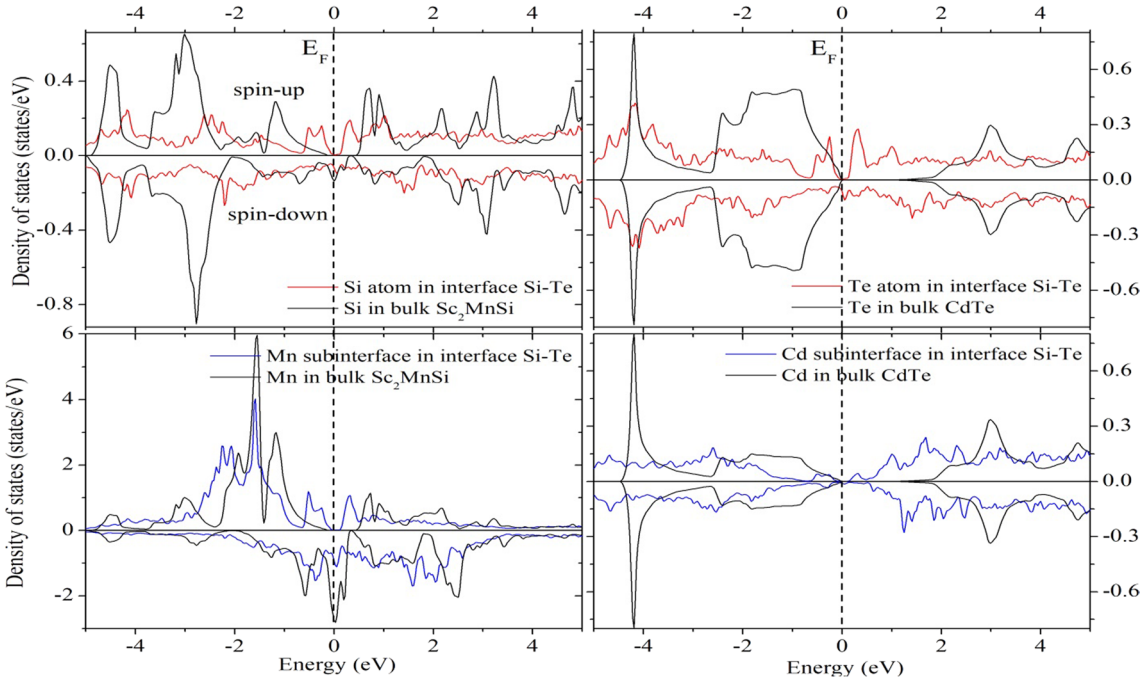

Fig. 11 The calculated density of states for the Si-Te shape of the Sc_2MnSi/CdTe (111) interface

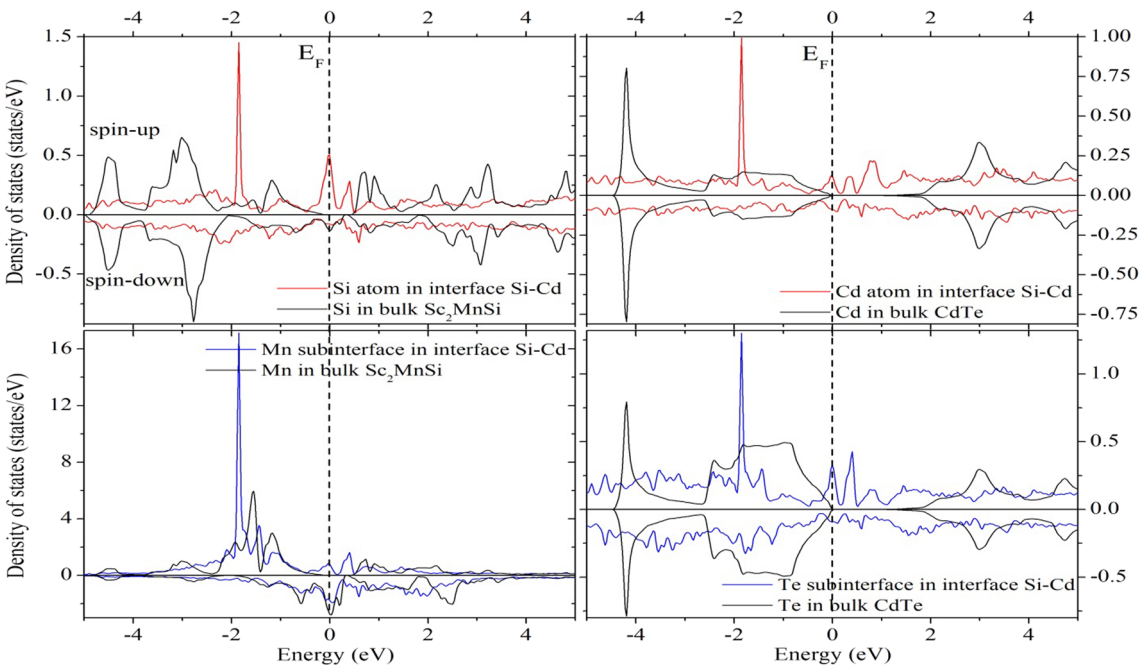

Fig. 12 The calculated density of states for the Si-Cd shape of the Sc_2MnSi/CdTe (111) interface

interfacial states as shown in Fig. 12. It indicates that the spin-up and spin-down electrons have metallic properties. To investigate the interface effect on the electronic and magnetic properties, the magnetic moments (M in μ_B) at the interface and sub-interface atoms are also revealed in Table 2. The matching bulk values are explained. Obviously, the M values of the interface atoms Si decreased compared to the bulk one because of the decreased spin splitting. Furthermore, we investigated the P of the interface and sub-interface atoms in all of the two distinct compositions stated in Table 2 in

Table 2 The atomic magnetic moments (in μ_B) and spin polarization (P) at the Si-Cd and Si-Te shapes, sub-interface (with *), and bulk full Heusler Sc_2MnSi alloy at the Sc_2MnSi/CdTe (111) interface

Interface structure	Magnetic moments (μ_B)				Spin polarization %			
	Si	Mn	Cd	Te	Si	Mn	Cd	Te
Si-Cd	−0.018	1.934*	−0.018	−0.039*	71.8	41.90*	16.93	37.75*
Si-Te	−0.047	2.328*	−0.001*	−0.018	100	100*	100*	100
Bulk	−0.05	2.09	0.00	0.00	100	100	0.00	0.00

Table 3 Illustrations the bond lengths (d_{int}) after relaxation. The needed information about the interfacial atoms and the adhesion energies (γ) including the two possible different shapes

Interfacial structure	d_{int} (Å)	γ (J m^{-2})
Si-Cd	3.36	0.87
Si-Te	3.30	1.96

order to better understand the importance of utilizing ferromagnetic materials as the base of the spin injection into semiconductors.

3.5 Adhesion energy and interface half-metallicity

In this part, an extensive study of the properties of the interface between the HM Sc_2MnSi and the semiconductor CdTe are revealed. The composition ZB because its lattice constant 6.477 Å is compatible with the lattice constant 6.34 Å of the Sc_2MnSi. Obviously, a CdTe semiconductor has two kinds of terminated, Cd-, and Te-terminated at the (111) surfaces, these terminations will merge with the Si-terminated for the Sc_2MnSi HM in the case of the (111) surfaces because of their retained HM properties. For this reason, the interfaces had two shapes in Sc_2MnSi/CdTe (111) with different arrangements which are as follows: Si-Cd, and Si-Te configurations. To study the Sc_2MnSi/CdTe (111) interface, the slabs built based on the following steps. The layers contain 25 of the HM Sc_2MnSi underneath 7 layers of the CdTe. The four atomic layers close to the Sc_2MnSi/CdTe interface are allowed to relax. In order to examine the stability of the Sc_2MnSi/CdTe interfacial structures, the adhesion energies will be calculated. The adhesion energy can be defined as the energy necessary to separate the interface into two free surfaces; therefore, it can be synonymous with the adhesion strength. The adhesive energy (γ) can be extracted from the following relationship [40, 41]:

$$\gamma = \left(E_{Sc_2MnSi} + E_{CdTe} - E_{Sc_2MnSi/CdTe}\right)/A,$$

where E_{Sc_2MnSi}, E_{CdTe} and $E_{Sc_2MnSi/CdTe}$ are the total energies of the Sc_2MnSi, CdTe and Sc_2MnSi /CdTe (111) slabs, respectively. A is the total interfacial area.

Table 3 displays the configurations of the Si-Cd/Si-Te interface. It is clear that there are an optimization in both the bonding lengths at o and the adhesion energies after relaxation. As shown in Table 3, it can be seen that the Si-Te configurations have the highest adhesion energies due to the least bond distance among the two configurations, while the Si-Cd have the lower adhesion energies due to the biggest bond distance. As a result, the Si-Te configuration is more stable than the other one.

4 Conclusions

To summarize briefly, the first-principles calculations were utilized to investigate the properties of the bulk Sc_2MnSi and the (111), (110), and (001) surfaces. These calculations included the Sc_2MnSi/CdTe (111) interface. It is clear that the HM properties are appearing in the Sc(2)Si-terminated (001), Sc2, Si-terminated (111) surfaces. On the contrary, the HM characteristic are destroyed for all Sc(1)Mn-terminated (001), Sc(1)-, Mn-(111), and Sc_2MnSi (110) surfaces. The HM properties of the bulk Sc_2MnSi lost their characteristic at the Sc_2MnSi/CdTe (111) interface. On the other hand, the Si-Te interface showed a full spin polarization, which made these materials a good candidate for upcoming spin electronics applications.

Author contributions MHJ wrote the first draft of the manuscript. JMKA-z has designed the study and analyzed data. All authors reviewed the final version of the manuscript.

Funding No funding was received.

Data availability There are no other data required.

Declarations

Conflict of interest The author declares that there is no conflict of interest.

References

1. S.S.P. Parkin, C. Kaiser, A. Panchula, P.M. Rice, B. Hughes, M. Samant, S.H. Yang, Nat. Mater. **3**, 862 (2004)
2. D.Z. Segu, P.V. Khan, P. Hwang, J. Mech. Sci. Technol. **32**, 3507 (2018)
3. S. Satoshi, H. Susumu, T. Masayuki, K. Yuzo, I. Hitoshi, Appl. Phys. Express **8**, 023103 (2015)
4. A. Kent, D. Worledge, Nat. Nanotech. **10**, 187 (2015)

5. A.K. Nayak, V. Kumar, T. Ma, P. Werner, E. Pippel, R. Sahoo, F. Damay, U.K. Rößler, C. Felser, S.S.P. Parkin, Nature **548**, 561 (2017)
6. S. Singh, S.W. D'souza, J. Nayak, E. Suard, L. Chapon, A. Senyshyn, V. Petricek, Y. Skourski, M. Nicklas, C. Felser, S. Chadov, Nat. Commun. **7**, 12671 (2016)
7. Y. Yang, Z.Y. Feng, J.M. Zhang, Superlat. Microstruct. **117**, 82 (2018)
8. M. Julliere, Phys. Lett. A **54**, 225 (1975)
9. Y. Chen, B. Wu, H. Yuan, Y. Feng, H. Chen, J. Solid State. Chem. **221**, 311 (2015)
10. T. Vasileiadis, L. Waldecker, D. Foster, A. Da Silva, D. Zahn, R. Bertoni, R.E. Palmer, R. Ernstorfer, ACS Nano **12**, 7710 (2018)
11. W. Bo, Y. Hongkuan, K. Anlong, F. Yu, C. Hong, J. Phys. D Appl. Phys. **44**, 405301 (2011)
12. X. Shen, G. Yu, C. Zhang, T. Wang, X. Huang, W. Chen, Phys. Chem. Chem. Phys. **20**, 15424 (2018)
13. T. Chen, J.H. Wang, Z.X. Cheng, X.T. Wang, H. Chen, Sci. Rep. **8**, 16530 (2018)
14. G. Yang, D. Li, S. Wang, Q. Ma, S. Liang, H. Wei, X. Han, T. Hesjedal, R. Ward, A. Kohn, J. Appl. Phys. **117**, 083904 (2015)
15. A. Xu, L. Shi, T. Zhao, Int. J. Heat Mass Transfer **126**, 753 (2018)
16. R. Grimm, S. Marchi, Earth Planet. Sci. Lett. **485**, 1 (2018)
17. N. Xing, Y. Gong, W. Zhang, J. Dong, H. Li, Comput. Mater. Sci. **45**, 4 (2009)
18. G.D. Liu, X.F. Dai, H.Y. Liu, J.L. Chen, Y.X. Li, Phys. Rev. B **77**, 014424 (2008)
19. H. Zenasni, H.I. Faraoun, C. Esling, J. Magn. Magn. Mater. **333**, 162 (2013)
20. H.Z. Luo, Z.Z. Zhu, L. Ma, S.F. Xu, H.Y. Liu, G.H. Wu, J. Phys, D Appl. Phys. **40**, 7121 (2007)
21. S. Kervan, N. Kervan, Intermetallics **24**, 56 (2012)
22. S. Kervan, N. Kervan, Intermetallics **37**, 88 (2013)
23. I. Galanakis, K. Özdoğan, E. Şaşıoğlu, B. Aktaş, Phys. Rev. B **75**, 172405 (2007)
24. J. Li, Y.X. Li, G.X. Zhou, Y.B. Sun, C.Q. Sun, Appl. Phys. Lett. **94**, 242502 (2009)
25. J.M. Khalaf Al-zyadi, H.I. Asker, K.L. Yao, Phys. E Low-Dimen. Syst. Nanostruct. **122**, 114196 (2020)
26. J.M. Khalaf Al-zyadi, A.H. Ati, K.L. Yao, J. Electron Spectrosc. Related Phenomena **244**, 146991 (2020)
27. J.M. Khalaf Al-zyadi, M.A. Nattiq, J.M. Al-Mukh, K.L. Yao, Solid State Commun. **314**, 113941 (2020)
28. J.M. Khalaf Al-zyadi, H.I. Asker, J. Electron Spectrosc. Related Phenomena **249**, 147060 (2020)
29. J.M. Khalaf Al-zyadi, A.H. Ati, K.L. Yao, Appl. Phys. A **126**(8), 1 (2020)
30. A. Bafekry, M.M. Obeid, C.V. Nguyen, M. Ghergherehchi, M. Bagheri Tagani, J. Mater. Chem. A **8**, 13248 (2020)
31. A. Bafekry, S. Karbasizadeh, M. Faraji, A. Bagheri Khatibani, I. AbdolhosseiniSarsari, D. Gogovae, M. Ghergherehchi, Phys. Chem. Chem. Phys. **23**, 21196 (2021)
32. A. Bafekry, M. Faraji, A. AbdollahzadehZiabari, M.M. Fadlallah, C.V. Nguyen, M. Ghergherehchi, S.A.H. Feghhi, New J. Chem. **45**, 8291 (2021)
33. M. Naseri, A. Bafekry, M. Faraji, D.M. Hoat, M.M. Fadlallah, M. Ghergherehchi, N. Sabbaghii, D. Gogova, Phys. Chem. Chem. Phys **23**, 12226 (2021)
34. A. Bafekry, C. Stampf, M. Ghergherehchi, Nanotechnology **31**, 295202 (2020)
35. A. Bafekry, M.M. Fadlallah, M. Faraji, A. Shafique, H.R. Jappor, I. AbdolhoseiniSarsari, Y.S. Ang, M. Ghergherehchi, Phys. Chem. Chem. Phys **24**, 9990 (2022)
36. A. Bafekry, D. Gogova, M.M. Fadlallah, N.V. Chuong, M. Ghergherehchi, M. Faraji, S.A.H. Feghhia, M. Oskoeian, Phys. Chem. Chem. Phys. **23**, 4865 (2021)
37. K. Schwarz, P. Blaha, Comput. Mater. **28**, 259 (2003)
38. F. Ahmadian, A. Salary Intermetallic **46**, 243 (2014)
39. S. Skaftouros, K. Özdogan, E. Şaşıoğlu, I. Galanakis, Phys. Rev. B **87**, 02442 (2013)
40. J.M. Khalaf Al-zyadi, G.Y. Gao, K.L. Yao, Comp. Mater. Sci. **86**, 140 (2014)
41. H. Luo, Z. Zhu, G. Liu, S. Xu, G. Wu, H. Liu, J. Qu, Y. Li, J. Magn. Magn. Mater. **320**, 421 (2008)